Numerical time-dependent solutions of the Schrödinger equation with piecewise continuous potentials

Wytse van Dijk*
Department of Physics, Redeemer University College, Ancaster, Ontario L9K 1J4, Canada
and Department of Physics and Astronomy, McMaster University, Hamilton, Ontario L8S 4M1, Canada
(Received 21 March 2016; published 15 June 2016)

We consider accurate numerical solutions of the one-dimensional time-dependent Schrödinger equation when the potential is piecewise continuous. Spatial step sizes are defined for each of the regions between the discontinuities and a matching condition at the boundaries of the regions is employed. The Numerov method for spatial integration is particularly appropriate to this approach. By employing Padé approximants for the time-evolution operator, we obtain solutions with significantly improved precision without increased CPU time. This approach is also appropriate for adaptive changes in spatial step size even when there is no discontinuity of the potential.

DOI: 10.1103/PhysRevE.93.063307

I. INTRODUCTION

As a fundamental equation of nonrelativistic quantum mechanics, the time-dependent Schrödinger equation has received considerable attention. In particular for nonrelativistic quantum mechanics the Schrödinger equation and its variants have a prominent place in investigating the atomic and subatomic world. The importance of these equations is evident from the plethora of applications in diverse areas of quantum mechanics.

While analytic solutions are desirable, and often preferred, the complexity of realistic systems inevitably leads to numerical approaches for obtaining them. There is a long history of developing and improving the numerical techniques of generating such solutions; see, e.g., Refs. [1–3]. Recently further sophistications have been introduced, and these have been scrutinized for their efficiency and accuracy, as well as their application to systems with time-dependent potentials or nonlinear interactions [4–8].

In 2007 we introduced a generalized Crank-Nicolson method (GCN) [3] by which one obtains accurate solutions in an efficient manner. An alternative method of choice developed by Talezer and Kosloff [2] involves the Chebyshev expansion of the time-evolution operator. Comparison of the two methods [9,10] indicates that the methods are comparable in efficacy; depending on the circumstances one performs better than the other. Unlike the Chebyshev expansion approach the GCN method is explicitly unitary.

Examples of the calculations which correspond to real systems abound in the literature. In the last few years one has found discussions, for example, involving the analysis of the Landau-Zener transitions in a spin-orbit coupled BEC [11], the numeric simulation of photoionization of many-electron atoms [12], the α-decay in ultra-intense laser fields [13], etc.

In this paper we consider numerical solutions to the one-dimensional time-dependent Schrödinger equation with different spatial step sizes in different regions of the computational space. Such step-size adaptation would allow for discontinuities of the potential or for efficient calculation by using small step sizes where there is much variation of the solution and large step sizes in regions of little to no variation. We use the Padé approximant expression for the time-evolution operator [3] and consider spatial subdomains within which equal steps are defined. For the spatial integration we perform a Numerov procedure [14]. The Numerov method, often used for stationary state equations, connects the wave function at three adjacent points, which makes it ideal for crossing points of changing step size. Furthermore the Numerov method is $O(h^6)$, where h is the spatial step size. This makes it more accurate than the three-point relation of the traditional Crank-Nicolson method.

The paper is organized so that Sec. II presents the general formulation, and Sec. III applies and evaluates the method using a superlattice consisting of square barriers. In Sec. IV the method is used for a numerical study of the decay of a particle through a δ-shell potential. Concluding comments are given in Sec. V.

II. GENERAL FORMULATION

We wish to determine the numerical solution of the time-dependent Schrödinger equation

$$H\Psi(x,t) = i\frac{\partial}{\partial t}\Psi(x,t), \quad \Psi(x,t_0) = \Phi(x), \tag{1}$$

where $\Phi(x)$ is the normalized wave function at initial time t_0. The time-independent Hamiltonian is

$$H = -\frac{\hbar^2}{2m}\frac{\partial^2}{\partial x^2} + V(x), \tag{2}$$

where $V(x)$ is the potential energy function with a finite number of discontinuities. The wave function at time $t + \Delta t$ is connected to the one at t by the time-evolution operator $\exp(-iH\Delta t/\hbar)$:

$$\Psi(x,t+\Delta t) = e^{-iH\Delta t/\hbar}\Psi(x,t). \tag{3}$$

We make a Padé-approximant expansion of the time-evolution operator [3]

$$e^{-iH\Delta t/\hbar} = \prod_{s=1}^{M} K_s^{(M)} + O[(\Delta)^{2M+1}], \tag{4}$$

*vandijk@physics.mcmaster.ca

where

$$K_s^{(M)} = \frac{1 + (iH\Delta t/\hbar)/z_s^{(M)}}{1 - (iH\Delta t/\hbar)/\bar{z}_s^{(M)}}. \tag{5}$$

The complex quantities $z_s^{(M)}, s = 1, \ldots, M$ are the zeros of numerator of the $[M/M]$ Padé approximant of the function e^z. We denote $\bar{z}$ as the complex conjugate of z. We discretize the time t so that $t_n = t_0 + n\Delta t, n = 0,1,2, \ldots$, so that

$$\Psi_{n+1} = e^{-iH\Delta t/\hbar}\Psi_n = \left(\prod_{s=1}^{M} K_s^{(M)}\right)\Psi_n + O[(\Delta t)^{2M+1}], \tag{6}$$

where $\Psi_n(x) = \Psi(x, t_0 + n\Delta t)$. As in our previous work [3] we find it convenient to calculate Ψ_{n+1} from Ψ_n iteratively by defining intermediate functions $\Psi_{n+s/M}, s = 0, \ldots, M$ such that

$$\Psi_{n+s/M} = K_s^{(M)}\Psi_{n+(s-1)/M}, \quad s = 1, \ldots, M. \tag{7}$$

Since $K_s^{(M)}$ are unitary operators, all intermediary functions are normalized.

At each stage of the problem the basic structure of the equation to be solved is

$$\psi(x, t - 2\Delta t/z) = \frac{1 + (iH\Delta t/\hbar)/z}{1 - (iH\Delta t/\hbar)/\bar{z}}\psi(x,t) \tag{8}$$

or

$$\left(1 - \frac{i\Delta t}{\hbar\bar{z}}H\right)y(x,t) = \left(\frac{1}{\bar{z}} + \frac{1}{z}\right)\psi(x,t), \tag{9}$$

where we have defined

$$y(x,t) = \frac{\psi(x, t - 2\Delta t/z)}{\bar{z}} + \frac{\psi(x,t)}{z} \tag{10}$$

and z is the generic $z_s^{(M)}$[15]. Note that $\sum_{s=1}^{M} \frac{1}{z_s^{(M)}} = -\frac{1}{2}$, so that after the M iterations of Eq. (7) the time advance is exactly Δt [4].

Equation (9) allows us to determine $\psi(x, t - 2\Delta t/z)$ from $\psi(x,t)$. This yields an equation of the type

$$y''(x,t) = g(x)y(x,t) + f(x,t) \tag{11}$$

for given t and $\Delta t/z$, where

$$g(x) = \frac{2m}{\hbar^2}V(x) + i\frac{2m\bar{z}}{\hbar\Delta t},$$
$$f(x,t) = -i\frac{2m\bar{z}}{\hbar\Delta t}\left(\frac{1}{\bar{z}} + \frac{1}{z}\right)\psi(x,t). \tag{12}$$

The double prime refers to the second partial derivative with respect to x. It should be noted that, although we are concentrating on the x dependence of the function $f(x,t)$, it also depends explicitly on t whereas $g(x)$ does not. If we consider a local partition of x, say, $\ldots, x_{j-1}, x_j, x_{j+1}, \ldots$, over a smooth region, we use the Numerov method to obtain a finite difference relation; i.e., since $y''(x_j) = g(x_j)y(x_j) + f(x_j)$ or $y_j'' = g_j y_j + f_j$ with $x_{j+1} - x_j = x_j - x_{j-1} = h$, we have

$$w_{j+1} = \left(2 + h^2\frac{g_j}{d_j}\right)w_j - w_{j-1} + h^2\frac{f_j}{d_j} + O(h^6), \tag{13}$$

where

$$w_j = d_j y_j - \tfrac{1}{12}h^2 f_j, \quad d_j = 1 - \tfrac{1}{12}h^2 g_j. \tag{14}$$

For convenience of the notation we have dropped the explicit t dependence; it is assumed that t remains constant. Hereafter we denote a point of discontinuity of the potential and a point at which the spatial step size changes, simply as a point of discontinuity. For the regions of x with no points of discontinuity we use the notation of Goldberg *et al.* [1] and Moyer [14]. The advantage of the Numerov method is that it yields a three-point difference formula, rather than the n-point formula of Refs. [3,10,16]. A three-point formula is convenient for crossing a point of discontinuity. Another useful feature of the Numerov method is that it leads to a result whose error is $O(h^6)$ as compared to $O(h^3)$ for the Crank-Nicolson method.

We now consider a partition over the full range of x values, i.e., $x_0, x_1, \ldots, x_{j-1}, x_j, x_{j+1}, \ldots, x_J$. We have chosen the partition so that the points of discontinuity occur at points x_s of the partition. For a proper solution we must ensure that both y and y' of Eq. (11) are continuous. In the following we let the step sizes change at $x = x_j = x_s$ and assume that the step size is h_- to the left of x_s and h_+ to the right of x_s. We make the following expansions:

$$y(x \pm h_\pm) = y(x) \pm h_\pm y'(x) + \frac{1}{2}h_\pm^2 y''(x) \pm \frac{1}{3!}h_\pm^3 y'''(x) + \frac{1}{4!}h_\pm^4 y^{iv}(x) \pm \frac{1}{5!}h_\pm^5 y^{v}(x) + O(h_\pm^6). \tag{15}$$

Using Eq. (11) and its derivatives we can express the higher-order derivatives of $y(x)$ in terms of $y(x)$ and $y'(x)$:

$$\begin{aligned} y'' &= gy + f, \\ y''' &= g'y + gy' + f', \\ y^{iv} &= (g'' + g^2)y + 2g'y' + gf + f'', \\ y^{v} &= (g''' + 4gg')y + (3g'' + g^2)y' + 3g'f + gf' + f'''. \end{aligned} \tag{16}$$

By defining $y_{s-1} = y(x_s - h_-)$ and $y_{s+1} = y(x_s + h_+)$ we obtain

$$y_{s\pm1} = E_s^\pm y_s - D_s^\pm y_s' + F_s^\pm, \tag{17}$$

where

$$\begin{aligned} D_s^- &= h_- + \frac{1}{6}h_-^3 g_s - \frac{1}{12}h_-^4 g_s' + \frac{1}{120}h_-^5\left(3g_s'' + g_s^2\right), \\ E_s^- &= 1 + \frac{1}{2}h_-^2 g_s - \frac{1}{6}h_-^3 g_s' + \frac{1}{24}h_-^4\left(g_s'' + g_s^2\right) \\ &\quad - \frac{1}{120}h_-^5(g_s''' + 4g_s g_s'), \\ F_s^- &= \frac{1}{2}h_-^2 f_s - \frac{1}{6}h_-^3 f_s' + \frac{1}{24}h_-^4(g_s f_s + f_s'') \\ &\quad - \frac{1}{120}h_-^5(3g_s' f_s + g_s f_s' + f_s'''). \end{aligned} \tag{18}$$

The expressions for D_s^+, E_s^+, and F_s^+ are obtained from the negative superscripted quantities in Eq. (18) by replacing h_- by $-h_+$. For D_s^+, E_s^+, F_s^+ all the derivatives and g_s are evaluated on the right of x_s and for D_s^-, E_s^-, F_s^- they are evaluated on the left of x_s. Since we use the three-point formula to step through the partition, whether we step from the right or from the left we reach the point x_s with value y_s. As we cross this point we begin a three-point recursion with this value of y_s, but also

need to have one of $y_{s\pm1}$ in order to restart the recursion. This quantity is obtained by demanding that y'_s is the same on both sides of x_s. From Eq. (17) we get

$$\frac{y_{s+1}-E_s^+y_s-F_s^+}{D_s^+}=\frac{y_{s-1}-E_s^-y_s-F_s^-}{D_s^-}. \tag{19}$$

This relation can be used to make the crossing of a point of discontinuity in either direction.

We use the recursion of w_j, Eq. (13), to obtain y_j:

$$y_j=\frac{w_j}{d_j}+\frac{1}{12}h^2\frac{f_j}{d_j}. \tag{20}$$

When $j=s$ we need to specify whether the quantities refer to the region $x\leqslant x_s$ or $x\geqslant x_s$ since $w(x)$ [unlike $y(x)$] is not continuous at x_s. Thus

$$\begin{aligned} w_s^{\pm}&=d_s^{\pm}y_s-\frac{1}{12}h_{\pm}^2f_s,\\ w_s^+&=w_s^-+(d_s^+-d_s^-)y_s-\frac{1}{12}(h_+^2-h_-^2)f_s,\\ w_s^-&=\frac{d_s^-}{d_s^+}w_s^+-\frac{1}{12}(d_s^+h_-^2-d_s^-h_+^2)\frac{f_s}{d_s^+}, \end{aligned} \tag{21}$$

where we have used $y_s=\frac{w_s^{\pm}}{d_s^{\pm}}+\frac{1}{12}h_{\pm}^2\frac{f_s}{d_s^{\pm}}$ to obtain the last equation. Writing Eq. (19) in terms of values of w, we obtain the connecting formula for w_s^+ and w_s^-:

$$\begin{aligned} &\frac{1}{D_s^+}\left[\frac{w_{s+1}}{d_{s+1}}+\frac{1}{12}h_+^2\frac{f_{s+1}}{d_{s+1}}-E_s^+\left(\frac{w_s^+}{d_s^+}+\frac{1}{12}h_+^2\frac{f_s}{d_s^+}\right)-F_s^+\right]\\ &\quad=\frac{1}{D_s^-}\left[\frac{w_{s-1}}{d_{s-1}}+\frac{1}{12}h_-^2\frac{f_{s-1}}{d_{s-1}}\right.\\ &\quad\left.-E_s^-\left(\frac{w_s^-}{d_s^-}+\frac{1}{12}h_-^2\frac{f_s}{d_s^-}\right)-F_s^-\right]. \end{aligned} \tag{22}$$

For the purpose of this paper we assume that the physical system is totally contained in the allotted space and that $\Psi(x_0,t)=\Psi(x_J,t)=0$. In that case it is convenient to reformulate the three-point relation of the w_j, Eq. (13), into two-point relations of two quantities e_j and q_j [1]. These quantities are defined through the relation

$$w_j=e_{j-1}w_{j-1}+q_{j-1}. \tag{23}$$

Where there is no point of discontinuity,

$$e_j=-\frac{1}{e_{j-1}}+2+h^2\frac{g_j}{d_j},\quad q_j=\frac{q_{j-1}}{e_{j-1}}+h^2\frac{f_j}{d_j}. \tag{24}$$

At a discontinuity,

$$w_{s+1}=e_s^+w_s^++q_s^+,\quad w_{s-1}=\frac{w_s^-}{e_{s-1}}-\frac{q_{s-1}}{e_{s-1}}. \tag{25}$$

Inserting these expressions into Eq. (22), we get an expression which includes linear terms in w_s^+ and w_s^-. Insertion of the last equation of Eq. (21) yields an equation which is linear in w_s^+ only. Equating the coefficients of w_s^+ we obtain an expression for e_s^+:

$$e_s^+=\frac{d_{s+1}}{d_s^+}\left[E_s^++\frac{D_s^+}{D_s^-}\left(\frac{d_s^-}{e_{s-1}d_{s-1}}-E_s^-\right)\right]. \tag{26}$$

The remaining terms in the equation, i.e., the coefficients of $(w_s^+)^0$, yield

$$\begin{aligned} q_s^+=&-\frac{1}{12}h_+^2f_{s+1}+\frac{1}{12}E_s^+h_+^2\frac{d_{s+1}}{d_s^+}f_s+d_{s+1}F_s^+\\ &+d_{s+1}\frac{D_s^+}{D_s^-}\left[-\frac{1}{12}\frac{1}{e_{s-1}d_{s-1}}(d_s^+h_-^2-d_s^-h_+^2)\frac{f_s}{d_s^+}\right.\\ &-\frac{q_{s-1}}{e_{s-1}d_{s-1}}+\frac{1}{12}h_-^2\frac{f_{s-1}}{d_{s-1}}-F_s^-\\ &\left.+\frac{1}{12}\frac{E_s^-}{d_s^-}(d_s^+h_-^2-d_s^-h_+^2)\frac{f_s}{d_s^+}-\frac{1}{12}E_s^-h_-^2\frac{f_s}{d_s^-}\right]. \end{aligned} \tag{27}$$

Given that the x integration is a two-point boundary condition problem, we start with $e_0=\infty$ [14] and $q_0=0$ since $\Psi(x_0,t)=0$ giving $w_0=0$. We then use the forward recursion, Eq. (24), until we reach the first point of discontinuity, x_s. We will have obtained e_s^- and q_s^-, from which we calculate e_s^+ and q_s^+ using Eqs. (26) and (27). These are used as initial values for further recursive evaluations using Eq. (24). We continue until we reach the next point of discontinuity and repeat the procedure until we reach e_{J-1} and q_{J-1}. Having obtained e_j,q_j, for $j=0,\ldots,J-1$, we follow with the backward recursion, $w_{j-1}=(w_j-q_{j-1})/e_{j-1}$, starting with $w_J=0$ since $\Psi(x_J,t)=0$. At a point of discontinuity we will have obtained $w_s^+=(w_{s+1}-q_s^+)/e_s^+$, and using the last of Eq. (21), we calculate w_s^-. We continue with the backward recursion until the next point of discontinuity, and repeat until we reach w_0. It should be noted that during the forward recursion we store e_s^+ and q_s^+ in memory since these are needed in the backward recursion. Because of the structure of the discontinuity relations we do not need e_s^- and q_s^-. In this way the numerical function $y(x,t)=\psi(x,t-2\Delta t)/\bar{z}+\psi(x,t)/z$ is obtained from w, and since $\psi(x,t)$ is the input, $\psi(x,t-2\Delta t/z)$ is determined.

III. APPLICATION OF THE METHOD TO SUPERLATTICES

Superlattices are layered structures by which particles (electrons) are reflected or transmitted. We consider the one-dimensional model of particle impinging normally on such structure. A simple example would be that of a simple seven-layered structure modeled by the potential

$$V(x)=\begin{cases}V_0, & d_1/2\leqslant|x|\leqslant d_1/2+d_2\\ V_0, & 3d_1/2+d_2\leqslant|x|\leqslant 3d_1/2+2d_2\\ 0, & \text{otherwise.}\end{cases} \tag{28}$$

This models a GaAs/AlGaAs superlattice with the barriers representing the AlGaAs layers and the wells the GaAs layers [17]. We choose parameters close to ones used in Refs. [17,18], i.e., $d_1=6.50$ nm, $d_2=2.54$ nm, $V_0=290$ meV, and $m=0.071m_e$, where m_e is the free electron mass.

A. Comparison of transmission probabilities from time-independent and time-dependent calculation

We allow wave packets with fairly sharp energy definition (hence very broad in space) to impinge on the superlattice. The computational space ranges from $-10\,000$ to $10\,000$ nm. The

initial wave function is

$$\Psi(x,0) = \frac{1}{\sqrt{\alpha\sqrt{2\pi}}} \exp\left[-(x-x_i)^2/(2\alpha)^2 + ik_0(x-x_i)\right], \tag{29}$$

where $x_i = -5000$ nm and $\alpha = 1000$ nm. Thus the spatial width of the packet is $\Delta x = 2\alpha = 2000$ nm, and the momentum uncertainty is $\Delta k = 0.0005$ nm^{-1}, giving an energy uncertainty of $\Delta E = 1.100 \times 10^{-3}$~nm$^{-2} = 8.384 \times 10^{-2}$ meV. The incident electrons have energies $E = 45, \ldots, 75$ meV in steps of 1 meV. We calculate the reflection and transmission probabilities as

$$R = \int_{x_0}^{-d} |\Psi(x,t_{\text{large}})|^2\, dx, \quad T = \int_{d}^{x_J} |\Psi(x,t_{\text{large}})|^2\, dx, \tag{30}$$

where $d = 3d_1/2 + 2d_2$ is the range of the potential region and t_{large} is a time large enough so that the wave function has become negligible in the potential region, but not so large that the transmitted and the reflected wave packets have reached the boundary of the computational space.

We also calculate the stationary state transmission and reflection probabilities by solving numerically the variable amplitude equations [19–21]

$$\begin{aligned} u'(x) &= 1 - 2iku(x) - 2mV(x)u(x)^2, \\ q'(x) &= -2ikq(x) - 2mq(x)V(x)u(x), \end{aligned} \tag{31}$$

where we integrate from the right of the potential region, from $a \geqslant d$ to $b \leqslant -d$ with the initial conditions $u(a) = (2ik)^{-1}$ and $q(a) = \exp(-2ika)/(2ik)$. The reflection and transmission amplitudes are, respectively,

$$\rho(k) = e^{2ikb}[2iku(b) - 1], \quad \tau(k) = 2ikq(b)e^{2ikb}. \tag{32}$$

These differential equations are straightforward to solve numerically, even with potential discontinuities, and yield very accurate solutions. In Fig. 1 we plot an continuous curve of $|\tau(k)|^2$ versus the energy, and we plot T as obtained from the time-dependent Schrödinger equation at discrete energies in the first transmission band. The agreement of the two calculations is excellent.

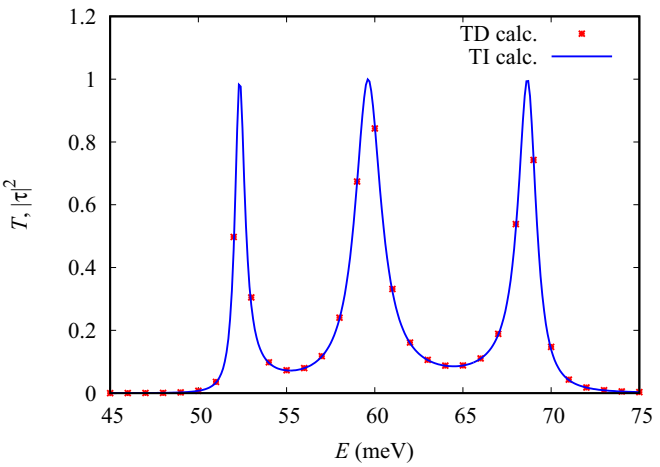

FIG. 1. Transmission coefficient calculated using the time-dependent (TD) and the time-independent (TI) calculations.

B. Wave function

It is instructive to make a detailed examination of the wave function at various times as the packet traverses the potential region. We consider a wave packet with energy near which total transmission occurs: $E = 54.2$ meV. In Fig. 2 we show the probability density at $t = 0{,}55dt{,}85dt{,}125dt$ where $dt = 15$. The wave packet evolves in time as it travels through the potential region. It is very wide compared to the range of the potential so that its energy spread is very small. Since we are near the resonance energy the wave packet becomes "trapped" in the potential region for a time and then emerges mostly as a transmitted packet. The tunneling time can be inferred by comparing the position of the transmitted packet to that of a packet that traveled through the same region when the potential is zero, i.e., the blue (leading) curve.

Of interest is the shape of the wave function that is in the potential region; it seems to have an unchanging shape, while its amplitude increases and decreases as the packet passes through the potential. The energy range shown in Fig. 1 corresponds to the first transmission band consisting of three peaks. The energy $E = 54.2$ meV corresponds to the energy of the first of these peaks. As the wave function is momentarily trapped, the wave function is approximately that of lowest (quasi-) bound state, i.e., the ground state when the outside barriers have infinite width.

C. Error calculations

The error can be defined as

$$(e_2)^2 \equiv \int_{x_0}^{x_J} dx\ |\Psi(x,t_1) - \Psi_{\text{exact}}(x,t_1)|^2, \tag{33}$$

which assumes the exact solution is known. In the case that the exact solution is not known, we could follow an approach where we compare the solution for a particular value of M to the one for $M+1$ [10] and define an error in terms of the difference of those solutions. However for our purpose here, we modify the definition of e_2 by considering the highest M-value approximation as the "exact" solution and define

$$(\eta_M)^2 \equiv \int_{x_0}^{x_J} dx\ |\Psi^{(M)}(x,t_1) - \Psi^{(M_{\max})}(x,t_1)|^2 \tag{34}$$

as an estimate of the accuracy of the solution. We consider again the wave scattering from the superlattice described in Eq. (28), but we use a narrower (in space) wave packet in order to reduce the computational space. For parameters we choose $\alpha = 10$, and $x_0 = -500$, $x_i = -200$, and $x_J = 500$, and we evaluate the wave function up to a maximum time of 90 units. In this case the energy range of the wave packet is large enough that the transmission is not unity, and the wave function in the potential does not display the symmetry behavior of Fig. 2. For an animation of the traveling wave packet, see Ref. [22]. To be specific, the space is divided into regions bounded by the discontinuities of the potential, as shown in Table I, where we list the numbers for the most accurate calculation, i.e., the lowest graph in Fig. 3. The quantity s labels the regions from left to right, n_s the number of spatial steps in region s, h_s the corresponding step size, and x_s the upper boundary of that region.

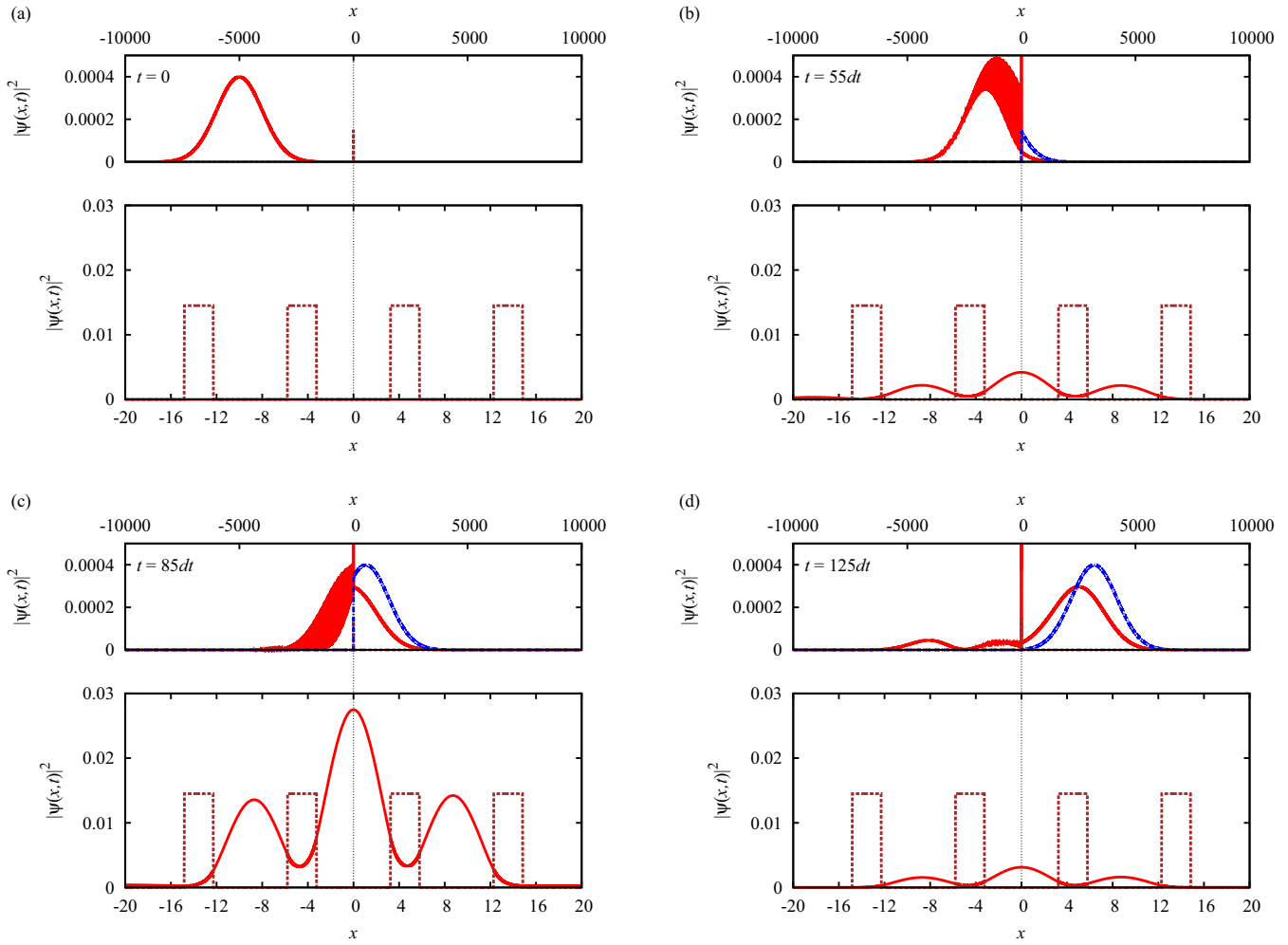

FIG. 2. The wave packet being scattered by the superlattice. Its energy is 52.4 meV; the distance units are nm, and $dt = 15$. The calculation employs $M = 10$. The solid red line represents the square of the magnitude of the wave function, the dash-dotted blue line is the magnitude of the square of the wave in the absence of the potential, and the dashed brown lines represent the superlattice potential. The time is indicated in each of the four subfigures. See Ref. [27] for an animation of this figure.

Figure 3 shows the errors as a function of M where we have chosen $M_{\max} = 20$. In each case we choose $dt = Mdt_0$. This ensures that on a particular graph points joined by a line correspond to calculations which take approximately the same CPU time. Remarkably one can obtain much more accurate solutions than the traditional $M = 1$ case, or even more so the traditional Crank-Nicolson calculation, with the

TABLE I. Parameters for the error calculations.

s	n_s	h_s	x_{s-1}	x_s
1	5,000	0.009703	−500	−14.83
2	250	0.010160	−14.83	−12.29
3	650	0.010000	−12.29	−5.79
4	250	0.010160	−5.79	−3.25
5	650	0.010000	−3.25	3.25
6	250	0.010160	3.25	5.79
7	650	0.010000	5.79	12.29
8	250	0.010160	12.29	14.83
9	5000	0.009703	14.83	500.00

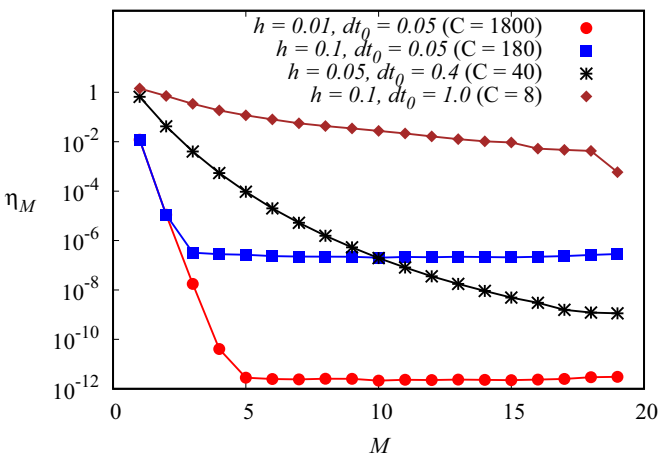

FIG. 3. Error as function of M. The parameters of the lowest curve are given in Table I. The other cases have numbers of intervals n_s divided by 2 or 10. The errors are calculated when $t = 90$. The symbol C refers to the approximate CPU time.

same computational effort. For the most accurate case shown the error is reduced by 10 orders of magnitude. Furthermore, in that case, even though we have chosen values of M up to 20, saturation sets in at around $M = 5$, and further increases of M do not lead to further improvement of the accuracy. The starred graph, however, is one in which the precision increases for every increase in M up to 20. An approximate relative CPU time is given for the calculation for each type of point on the graph. Where two curves intersect one could select the more precise calculation with the smaller CPU time. The one such point on the graph shows a possible reduction in CPU time by at least a factor of four. Exploration of the input parameters allows one to optimize the precision and computational efficiency.

IV. DECAY THROUGH A δ-FUNCTION BARRIER

A system which has a discontinuous potential resulting in a discontinuity of the spatial derivative of the wave function is the δ-function potential. A simplified model of α decay has a particle initially trapped in the S partial wave of an infinite square well of radius a. At $t = 0$ the well is replaced by a repulsive δ-shell potential at the square well's edge [23,24]. In this three-dimensional system the calculation is limited to the S-state partial wave for which the potential is

$$V(r) = \frac{\hbar^2}{2ma}\lambda\delta(r-a) \qquad \text{for} \qquad r \geqslant 0. \tag{35}$$

Then Eq. (11) generates a discontinuity condition at $r = a$,

$$y'(a_+,t) - y'(a_-,t) = \frac{\lambda}{a}y(a,t), \tag{36}$$

which in fact replaces the potential. Equation (19) becomes

$$\frac{y_{s+1} - E_s^+ y_s - F_s^+}{D_s^+} = \frac{y_{s-1} - E_s^- y_s - F_s^-}{D_s^-} + \frac{\lambda}{a}y_s \tag{37}$$

when $r_s = a$ and retains its original form for other values of s where the step length changes.

In order to compare the numerical results to the analytic ones of Refs. [24,25], we set $\hbar = 1$ and $m = 1/2$. The model parameters are $a = 1$ and $\lambda = 3$. The initial wave function is

$$\psi(r,0) = \phi_k(r) \equiv \sqrt{2/a}\,\sin(k\pi r/a)\theta(a-r)\theta(r), \tag{38}$$

where k is a natural number. It should be noted that for the S partial wave $\psi(0,t) = 0$ for all t. The wave functions for $t = 3$, a time much longer than the half-life, are in good agreement [26] as is evident in Fig. 4. In fact, the graphs of the numerical and analytic solutions are indistinguishable. We calculate the error using expression (33) where the exact solution is the analytic one given in Refs. [24,25]. The error is $e_2 = 8 \times 10^{-3}$. Actually the analytic solution consists of series over the zeros of the Jost function (or poles of the S matrix). The series do not converge very rapidly; in our calculation we allow up to one million poles to contribute. We also calculate $\eta_{19} = 1 \times 10^{-3}$, where $M_{\max} = 20$, indicating that the precision of the numerical solution in this case is greater than the analytic solution with a finite (but large) number of terms in the series.

In Fig. 5 we show the propagation of the escaping wave packet at increasing times.

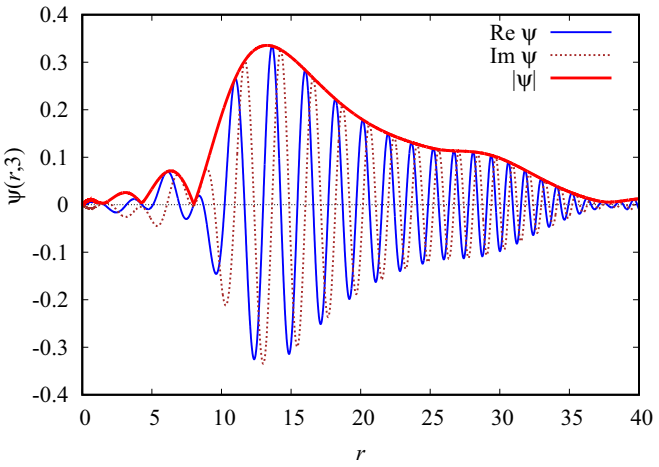

FIG. 4. The real part, the imaginary part, and the absolute value of the wave function in the region where it is dominant at time $t = 3$. The parameters of the system are $\lambda = 3$, $a = 1$, and $k = 1$.

The horizontal axis is a logarithmic scale. With increasing time the maximum amplitude of the packet decreases and its width increases. The Supplemental Material includes a animation of the time evolution of the decaying wave packet [27].

We also calculate the nonescape and survival probabilities as a function of time:

$$P_{\text{ne}}(t) = \int_0^a |\psi(r,t)|^2\,dr,$$
$$P_{\text{surv}}(t) = \left|\int_0^a \psi(r,0)\psi(r,t)\,dr\right|^2. \tag{39}$$

The curves shown in Fig. 6 are typical for a system like this [25]. The exponential decay dominates the process for the initial five or so half-lives; the half-life for the system $T_{1/2}$ is

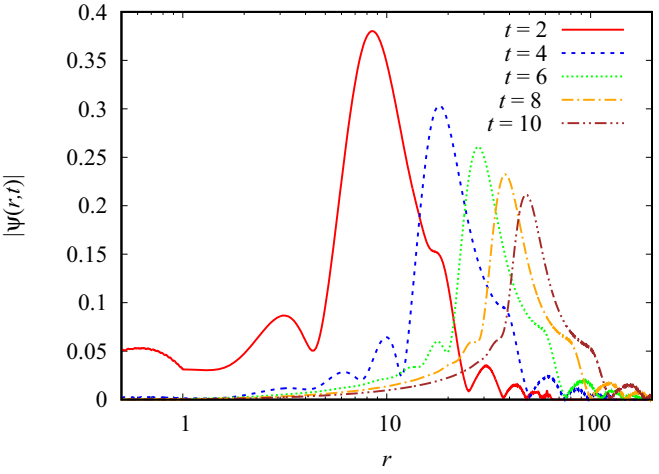

FIG. 5. The magnitude of the wave function at increasing times. Note that logarithmic scale along the horizontal axis. The parameters of the system are $\lambda = 3$, $a = 1$, and $k = 1$. See Ref. [27] for an animation of this figure.

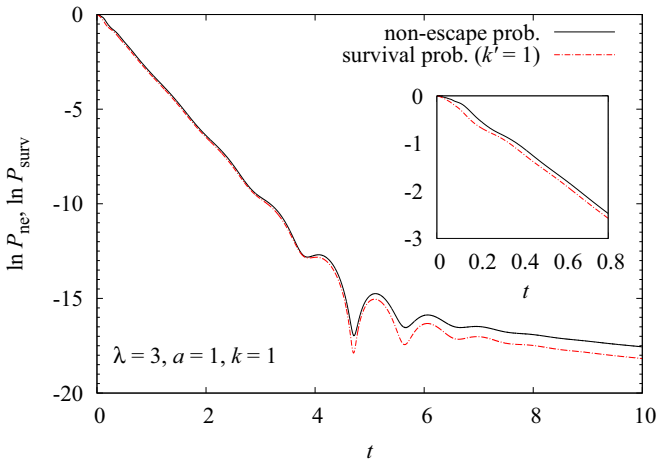

FIG. 6. Nonescape and survival probabilities as a function of time when $\lambda = 3$ and $a = 1$. The initial state has $k = 1$.

approximately 0.638 time units. Then as the system transitions from exponential decay to inverse power decay law, i.e., t^{-3}, there is significant fluctuation, which means, remarkably, that the current is negative for short times. The sign reversal of the current indicates that at certain times the particle probability inside the potential region increases. This feature was pointed out in Ref. [23].

The initial wave function is an eigenstate of the infinite square well potential. The ground state corresponds to $k = 1$, the first excited state to $k = 2$, etc. Thus if we consider $k = 2$ for the initial state, the system starts out with higher energy. The decay curves for such a system are shown in Fig. 7. The system decays out of the excited state and, besides generating an outgoing wave, it also populates the ground state. When there still is an appreciable excited-state component the decay rate is relatively fast; when it is depleted the system decays from the ground state much with the same characteristics as if it had started from the ground state. One obtains two different exponential decay curves with some fluctuation when

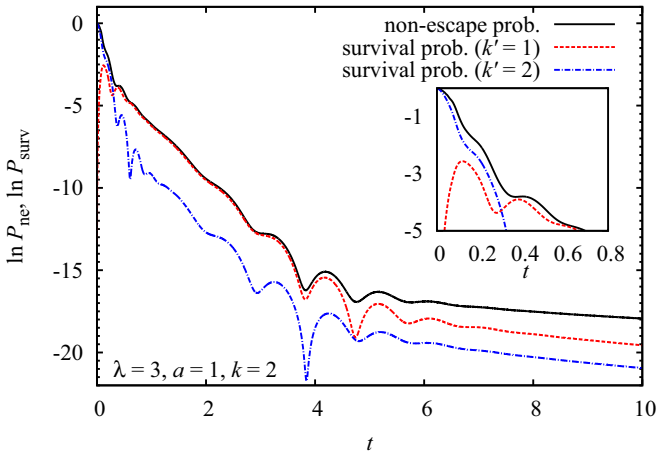

FIG. 7. Nonescape and survival probabilities when $k = 2$. The inset gives the graph zoomed in for small times. Note that it also shows the probability of the particle being in state $\phi_1(r)$ as a function of time.

the system switches from one exponential decay relation to the other. Similar behavior was shown in an exact calculation by Garcia-Caldéron *et al.* [28].

V. CONCLUSION

The Padé approximant of the time-evolution operator combined with Numerov method of spatial integration provides an approach for determining accurate solutions of the time-dependent Schrödinger equation. Interestingly the precision can be improved over the traditional Crank-Nicolson method by more than 10 orders of magnitude using approximately the same amount of computing resources, i.e., memory and CPU time.

The applications display results for simple models. However, there is no reason that for more realistic calculations, such as those including antireflecting coatings for the superlattices (see, e.g., Refs. [18,29,30]), the results would be less precise. A similar statement can be made about the decaying quantum system. More complicated barriers of finite width would be amenable to the analysis of this paper.

It should be noted that the approach, in principle, does not limit the number of discontinuities of the potential in computational space. To be practical, however, there needs to be a finite distance between adjacent discontinuities. Thus the restriction on the number of discontinuities of the potential is that there are at most a countable infinity of them.

To reduce computational effort one often introduces transparent boundary conditions at the edge of the computational space, so that wave packets are allowed to exit without reflection and altering the wave function in the region of interest [14,31,32]. We have not used such conditions because we wanted to study the wave function outside the potential region, especially for the decaying systems. Nevertheless, the numerical method allows us to investigate the transparent boundary conditions especially when there is a fluctuating current at potential edge. We leave this for future consideration.

Further investigation will deal with the application of the method to two- or three-dimensional systems using the Alternating Direction Implicit method of Peaceman and Rachford [33]. The applicability of the method to multichannel problems [34] and nonlinear and time-dependent potentials [4] is also a topic of later study. In particular the study of an equation with a cubic nonlinearity may be of interest for BEC under a superlattice. In Ref. [4] it is shown that the nonlinear term could be included as a nonhomogeneous term and equations like Eq. (8) result with ψ containing an additive term which depends on the wave function. A self-consistent iterative procedure was shown to be feasible. This is a natural and significant extension of the current research with discontinuous potentials.

ACKNOWLEDGMENT

The author would like to thank Prof. Y. Nogami for helpful discussions.

[1] A. Goldberg, H. M. Schey, and J. L. Swartz, Am. J. Phys. **35**, 177 (1967).

[2] H. Tal-Ezer and R. Kosloff, J. Chem. Phys. **81**, 3967 (1984).

[3] W. van Dijk and F. M. Toyama, Phys. Rev. E **75**, 036707 (2007).

[4] W. van Dijk and F. M. Toyama, Phys. Rev. E **90**, 063309 (2014).

[5] X. Liang, A. Q. M. Khaliq, and Q. Sheng, Appl. Math. Comput. **235**, 235 (2014).

[6] M. Ndong, H. Tal-Ezer, R. Kosloff, and C. P. Koch, J. Chem. Phys. **132**, 064105 (2010).

[7] E. Doha, A. Bhrawy, M. Abdelkawy, and R. A. Van Gorder, J. Comput. Phys. **261**, 244 (2014).

[8] L. W. Zhang and K. M. Liew, Appl. Math. Comput. **249**, 333 (2014).

[9] M. Formánek, M. Váňa, and K. Houfek, in *Numerical Analysis and Applied Mathematics, International Conference 2010*, edited by T. E. Simos, G. Psihoyios, and C. Tsitouras (American Institute of Physics, New York, 2010), p. 667.

[10] W. van Dijk, J. Brown, and K. Spyksma, Phys. Rev. E **84**, 056703 (2011).

[11] A. J. Olson, S.-J. Wang, R. J. Niffenegger, C.-H. Li, C. H. Greene, and Y. P. Chen, Phys. Rev. A **90**, 013616 (2014).

[12] D. Hochstuhl, C. M. Hinz, and M. Bonitz, Eur. Phys. J. Special Topics **223**, 177 (2014).

[13] Ş. Mişicu and M. Rizea, J. Phys. G: Nucl. Part. Phys. **40**, 095101 (2013).

[14] C. A. Moyer, Am. J. Phys. **72**, 351 (2004).

[15] There is an alternative approach, which may be slightly more efficient computationally. Since the set $\{z_s^{(M)}\}$ are the zeros of a polynomial, each complex $z_s^{(M)}$ also has its complex conjugate as a member of the set. Thus we can define $L_s^{(M)} = \frac{1+(iH\Delta t/\hbar)/z_s^{(M)}}{1-(iH\Delta t/\hbar)/z_s^{(M)}}$, which gives $\prod_{s=1}^{M} L_s^{(M)} = \prod_{s=1}^{M} K_s^{(M)}$. The $K_s^{(M)}$ are each unitary operators, whereas the $L_s^{(M)}$ are not. However, the full operator which is the product of all the $K_s^{(M)}$, or of all the $L_s^{(M)}$, is unitary, and hence it preserves the normalization. In this case the basic equation is

$$\psi(x,t+\Delta t/z) = \frac{1+(iH\Delta t/\hbar)/z}{1-(iH\Delta t/\hbar)/z}\psi(x,t),$$

which leads to an equation like Eq. (11) with

$$g(x) = \frac{2m}{\hbar^2}V(x) + i\frac{2mz}{\hbar\Delta t}, f(x,t) = -i\frac{4mz}{\hbar\Delta t}\psi(x,t).$$

.

[16] H. Shao and Z. Wang, Phys. Rev. E **79**, 056705 (2009).

[17] C. Pacher, W. Boxleitner, and E. Gornik, Phys. Rev. B **71**, 125317 (2005).

[18] C. Pacher and E. Gornik, Phys. Rev. B **68**, 155319 (2003).

[19] Y. Tikochinsky, Ann. Phys. (NY) **103**, 185 (1977).

[20] W. van Dijk and M. Razavy, Int. J. Quant. Chem. **16**, 1249 (1979).

[21] W. van Dijk and M. Razavy, Can. J. Phys. **57**, 1952 (1979).

[22] The characteristics of the scattering are shown in the animation [27].

[23] R. G. Winter, Phys. Rev. **123**, 1503 (1961).

[24] W. van Dijk and Y. Nogami, Phys. Rev. Lett. **83**, 2867 (1999).

[25] W. van Dijk and Y. Nogami, Phys. Rev. C **65**, 024608 (2002).

[26] Note that in Ref. [25] there should a minus sign in front of Eqs. (33) and (36) .

[27] See Supplemental Material at http://link.aps.org/supplemental/10.1103/PhysRevE.93.063307 for animations of Figs. 2 and 5.

[28] G. García-Caldéron, J. L. Mateos, and M. Moshinsky, Phys. Rev. Lett. **74**, 337 (1995).

[29] C. Pacher and E. Gornik, Physica E **21**, 783 (2004).

[30] C. N. Veenstra, W. van Dijk, D. W. L. Sprung, and J. Martorell, arXiv:cond-mat/0411118 (2006).

[31] V. Baskakov and A. Popov, Wave Motion **14**, 123 (1991).

[32] R. M. Feshchenko and A. V. Popov, Phys. Rev. E **88**, 053308 (2013).

[33] D. W. Peaceman and J. H. H. Rachford, J. Soc. Indust. Appl. Math. **3**, 28 (1955).

[34] W. van Dijk, K. Spyksma, and M. West, Phys. Rev. A **78**, 022108 (2008).